Modeling and Simulation of Magnetic Shape-Memory Polymer Composites

Sergio Conti, Martin Lenz, Martin Rumpf

no. 299

Diese Arbeit ist mit Unterstützung des von der Deutschen Forschungsgemeinschaft getragenen Sonderforschungsbereiches 611 an der Universität Bonn entstanden und als Manuskript vervielfältigt worden.

Bonn, Oktober 2006

Modeling and simulation of magnetic shape-memory polymer composites

September 7, 2006

S. Conti[1], M. Lenz[2], M. Rumpf[2]

[1] *Fachbereich Mathematik, Universität Duisburg-Essen, Lotharstr. 65, 47057 Duisburg, Germany*

[2] *Institut für Numerische Simulation, Universität Bonn, Nussallee 15, 53115 Bonn, Germany*

Composites of small magnetic-shape-memory (MSM) particles embedded in a polymer matrix have been proposed as an energy damping mechanism and as actuators. Compared to a single crystal bulk material, the production is simpler and more flexible, as both type of the polymer and geometry of the microstructure can be tuned. Compared to polycrystals, in composites the soft polymer matrix permits the active grains to deform to some extent independently; in particular the rigidity of grain boundaries arising from incompatible orientation is reduced. We study the magnetic-field-induced deformation of composites, on the basis of a continuous model incorporating elasticity and micromagnetism, in a reduced two-dimensional, plane strain setting. The aim is to give conceptual guidance for the design of composite materials independent of the concrete macroscopic device. Thus on the background of homogenization theory, we determine the macroscopic behaviour by studying an affine-periodic cell problem. An energy descent algorithm is developed, whose main ingredients are a boundary element method for the computation of the elastic and magnetic field energies; and a combinatorial component reflecting the phase transition in the individual particles, which are assumed to be of single–domain type. Our numerical results demonstrate the behavior of the macroscopic material properties for different possible microstructures, and give suggestions for the optimization of the composite.

AMS Subject Classifications (2000): 74Q05, 74N05, 65N38

1 Introduction

Ferromagnetic shape-memory materials exhibit comparably large strains in response to an applied magnetic field. For single crystals one can achieve strains of order of magnitude 10% [41, 39, 27, 38]. In polycrystals the effectivity drops significantly, as a consequence of the rigidity of interacting grains [1, 40].

A recently-proposed alternative for shape memory devices is to embed small single-crystal shape-memory particles in a soft polymer matrix [16, 17]. This approach gives a large freedom in the material development, which includes the type of polymer, the density of particles, their shape, their orientation [36]. In the case of classical magnetostrictive materials, such as Terfenol-D, experiments have shown that using elongated particles, and orienting them via a bias field during solidification of the polymer, leads to a much larger magnetostriction of the composite [35, 31]. Some analytical models have been proposed to estimate the effect of the geometric configuration, focussing in the dilute limit and with simple geometries of the particles: Feng, Fang and Hwang developed a Green's function approach for dilute magnetostrictive composites containing ellipsoidal particles [15]; and Liu, James and Leo studied a similar geometry with MSM particles, that were treated with a constrained theory [24]. Quantitative predictions for generic geometries are, however, still missing. A first numerical analysis based on an interface-enriched reproducing kernel method was presented in [42].

We present here a systematic approach to the quantitative determination of macroscopic material properties of magnetostrictive–polymer composites. In Section 2 we develop a general continuous model, which incorporates elasticity and micromagnetism. We consider a soft elastic polymer with small embedded magnetic shape-memory (MSM) particles. The latter have two phases, indexed by a discrete parameter, with different spontaneous deformations and different magnetic anisotropies; the phase index is assumed constant inside each particle. Both eigenstrain and anisotropy have an orientation which depends on the local crystal lattice orientation. The particles interact with the external magnetic field via a Zeeman term, and with each other via the demagnetization field, as well as via the elastic deformation of the polymer matrix. In Section 3 we discuss homogenization of the model, based on results from homogenization theory [43, 30, 6, 9]. Assuming that the particles are much smaller than the sample size, and that the microstructure is periodic, the problem effectively decouples in a macroscopic part, which depends on the sample geometry and the spatial variation of the applied field, and a microscopic part, which depends on the microstructure. We focus here on the latter, and show how its numerical solution permits to obtain the

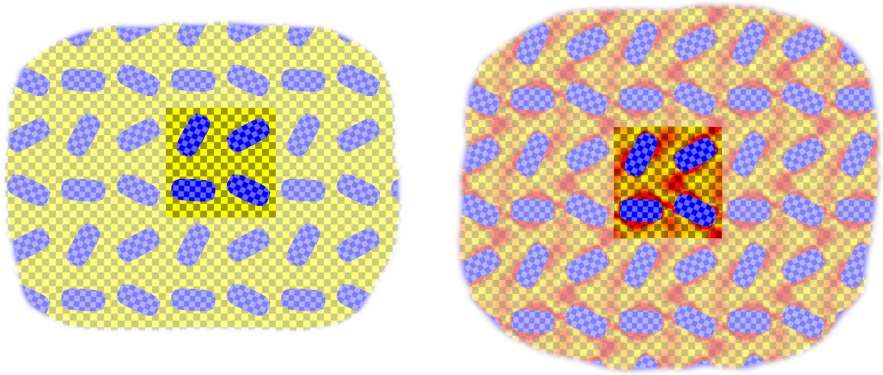

(a) (b)

FIGURE 1: Reference configuration (a) and deformed configuration (b) for a periodic composite, containing particles with four different orientations. For illustrative purposes, a finite portion of a periodic lattice is plotted, with the computational cell in the center. The checkerboard pattern illustrates the elastic deformation, the color coding the strain in the matrix. A detailed description can be found in Section 6 below.

effective macroscopic energy density, which enters the macroscopic problem. This way we can understand how one can tune the effective material properties by varying the microstructure. In turn, the macroscopic problem can be solved analytically in simple geometries. A future goal is to base macroscopic device simulations on material properties derived on the microscale.

Our algorithm and the numerical simulations are based on periodic cell problems in a plane strain, two–dimensional setting; each particle is assumed to have a uniform magnetization and strain, see Figure 1 for an illustration. The numerical computations are performed with linear elasticity, which is admissible since the expected material deformation is in the range of some percent. Beyond that, it enables a treatment by a boundary element method. Based on combinatorial testing, we then minimize over all possible values of the phase index. We investigate the macroscopic material behavior depending on the volume fraction of MSM particles in the polymer lattice, the distribution of their orientations, the aspectratio of particle shapes, and the elastic moduli of the polymer.

Previous theoretical modeling of single-crystal magnetic-shape-memory and magnetostrictive single-crystals, on which the model presented in Section 2 is partially based, can be found in [13, 19, 29, 39, 23, 14]. For a more detailed explanation of the elastic modeling of phase-transforming materials we refer to [4]. For simplicity we only discuss the model in two dimensions,

the extension to three dimensions is straightforward. The model considered here can be extended to polycrystals (seen as a limit where the particles fill all space), see [11].

2 Micromagnetic-elastic model

Let $\Omega \subset \mathbb{R}^2$ be the domain occupied by the composite, and let $\omega \subset \Omega$ denote the part occupied by the active material. From an elastic viewpoint, $\Omega \setminus \omega$ is occupied by a purely elastic, isotropic material, and ω represents a shape-memory material, which has two phases (called 1 and 2 below) with different eigenstrains (see (2.2) below). Furthermore, the material in ω is magnetic, with different preferred anisotropies in the two phases. The kinematic variables and the terms composing the energy are illustrated below.

Kinematics. Let $v : \Omega \to \mathbb{R}^2$ be the elastic deformation, $p : \omega \to \{1, 2\}$ be the phase index, which is supposed to be constant on each single particle, and $M : \mathbb{R}^2 \to \mathbb{R}^2$ the magnetization. Notice that v and p are defined on the reference configuration, whereas M is defined on the deformed configuration (i.e., v and p are material fields, M is a spatial field). Precisely, a material point $x \in \Omega$ is mapped to the point $v(x) \in \mathbb{R}^2$ under the deformation, its phase is $p(x)$, and its magnetization is $M(v(x))$. We assume v to be injective on Ω, which in particular corresponds to a non-interpenetration condition for the MSM particles. Since the polymer matrix is not magnetic, we suppose M to vanish outside the particles, i.e., $\operatorname{supp} M = v(\omega)$.

Elasticity. The elastic energy of the polymer matrix takes the general form

$$E^{\text{elast}}_{\text{matr}}[v] = \int_{\Omega\setminus\omega} W_{\text{matr}}(\nabla v(x))\, dx\,,$$

where $W_{\text{matr}} : \mathbb{R}^{2\times 2} \to [0, \infty]$ is the stored energy density of the matrix. The particles have two energy-minimizing phases, which are distinguished by the phase parameter p, and are elastically anisotropic. Thus, we write their elastic energy as

$$E^{\text{elast}}_{\text{part}}[v, p] = \int_{\omega} W_{\text{part}}((\nabla v(x))Q(x), p(x))\, dx\,. \tag{2.1}$$

Here $Q : \omega \to SO(2)$ represents the crystal lattice orientation in the reference configuration, and the energy density $W_{\text{part}}(F, p)$ penalizes deviations from a preferred, phase-dependent, strain. Qualitatively,

$$W_{\text{part}}(F, p) \simeq \operatorname{dist}^2 (F, SO(2)\,(\mathrm{Id} + \varepsilon_p))\ ,$$

where ε_p is the eigenstrain of phase p, say,

$$\varepsilon_1 = \begin{pmatrix} -\varepsilon_0 & 0 \\ 0 & \varepsilon_0 \end{pmatrix}, \qquad \varepsilon_2 = \begin{pmatrix} \varepsilon_0 & 0 \\ 0 & -\varepsilon_0 \end{pmatrix}. \tag{2.2}$$

A precise expression for $W_{\rm part}$, incorporating appropriate elastic constants, will be given below. Notice that the lattice rotation is inserted explicitly through Q, hence $W_{\rm part}(F,p)$ is taken with respect to a canonical lattice orientation, i.e., it is the same function for all particles.

Micromagnetism. Let $M = M_s m$ be the magnetization, where M_s denotes the saturation magnetization. The vector field $m : \mathbb{R}^2 \to \mathbb{R}^2$ satisfies

$$|m|(y) = \begin{cases} 1 & \text{if } y \in v(\omega)\,, \\ 0 & \text{else.} \end{cases} \tag{2.3}$$

We stress that the magnetization is defined on the deformed configuration, which is the one where Maxwell's equations hold; to make the distinction clear we use y as an independent variable on the deformed configuration. Since v is injective on ω, instead of m as in (2.3) we can equivalently consider a unit length vector field $\tilde{m}$ on ω and set $m = \tilde{m} \circ v^{-1}$; for simplicity we shall stick to the first formulation. Thus, the admissible values of m depend on the deformed configuration and thus on the deformation; we express this fact by making all components of the magnetic energy depend on v.

The magnetic energy is given by the coupling to the external field $H_{\rm ext}$,

$$E_{\rm ext}[v,m] = -\frac{M_s}{\mu_0} \int_{\mathbb{R}^2} H_{\rm ext} \cdot m \, dy\,,$$

μ_0 being the vacuum permeability constant, and the demagnetization term

$$E_{\rm demag}[v,m] = \frac{M_s^2}{\mu_0} \int_{\mathbb{R}^2} \frac{1}{2} |H_d|^2 dy\,,$$

see, e.g., [3, 18]. The field $H_d : \mathbb{R}^2 \to \mathbb{R}^2$ is the projection of m onto curl-free fields, i.e., $H_d = \nabla\psi$, where $\psi : \mathbb{R}^2 \to \mathbb{R}^2$ is the solution of

$$\Delta\psi = \operatorname{div} m \tag{2.4}$$

in a distributional sense. Corresponding to the two different eigenstrains, the two phases of the shape-memory material are assumed to have different magnetic anisotropies, and the easy axis is in both cases oriented along the compressive direction of the eigenstrain. Precisely, we take into account

$$E_{\rm anis}[v,m,p] = K_u \int_{v(\omega)} \varphi_{p(v^{-1}(y))} \left((R_{\nabla v \circ v^{-1}} Q(y))^T m \right) dy\,.$$

Here, $\varphi_2(m) = \frac{m_1^2}{|m|^2}, \varphi_1(m) = \frac{m_2^2}{|m|^2}$ are the two magnetic anisotropy functions reflecting the phase–dependent easy axis, Q and p are the lattice orientation and the phase field, as in (2.1), and K_u is the uniaxial anisotropy constant, with dimensions of energy per unit volume. The matrix $R_{\nabla v(x)} \in SO(2)$ is the rotation associated with the elastic deformation v at a reference point x. It is defined via the polar decomposition, i.e.,

$$R_F = F(F^T F)^{-1/2}\,. \tag{2.5}$$

Since m is a spatial field, the combination $R^T m$ is frame indifferent. The full expression $Q^T R^T m$ gives the pull-back of the direction of m to a lattice with the reference orientation, under the action of the rotational part alone of the deformation gradient.

Finally, the exchange energy takes the form

$$E_{\text{exch}}[v, m] = \frac{1}{2} d^2 \int_{v(\omega)} |\nabla m|^2 dy\,.$$

Here d is the exchange length, i.e., the length scale below which the exchange effects modeled by E_{exch} become relevant. In the limit of small particles, where we assume constant magnetization on single particles and thus $\nabla m = 0$ on ω, the exchange energy vanishes.

Combining the different energy contributions we obtain the full model in the general case:

$$\begin{aligned} E[v, m, p] \;=\; & E^{\text{elast}}_{\text{matr}}[v] + E^{\text{elast}}_{\text{part}}[v, p] + E_{\text{ext}}[v, m] \\ & + E_{\text{demag}}[v, m] + E_{\text{anis}}[v, m, p] + E_{\text{exch}}[v, m]\,. \end{aligned}$$

3 Homogenization

In the case relevant for the applications the number of particles is very large, and each particle is very small. Thus, a direct simulation of larger scale particle ensembles is not feasible. In the spirit of the theory of homogenization [43, 30, 6, 9, 26], we study periodic configurations, where each periodic cell contains a small number of particles, as illustrated in Figure 1. We assume the microstructure to be periodic, and obtained by downscaling a fixed microstructure defined on the unit square $Q = (0, 1)^2$, assuming for simplicity that the MSM particles do not intersect the boundary, i.e., $\omega = \cup \omega_i \subset Q$ (see Fig. 1). From now on ω denotes only the part of magnetic material inside the unit cell. Let ε be the scale of the microstructure. We consider the

family of problems defined on a fixed domain $\Omega \subset \mathbb{R}^2$, where the magnetic particles cover

$$\omega_\varepsilon = \left\{ x \in \Omega : \frac{x}{\varepsilon} \in \omega + \mathbb{Z}^2 \right\},$$

and the polymer the complement, $\Omega \setminus \omega_\varepsilon$. The full problem involves minimizing the full energy E over fields $v : \Omega \to \mathbb{R}^2$, and $m : \mathbb{R}^2 \to \mathbb{R}^2$ with $|m| = 1$ on $v(\omega_\varepsilon)$ (as above, we tacitly assume v to be invertible). The theory of homogenization is based on the idea of separating in the limit $\varepsilon \to 0$ the microscopic scale, which resolves the microstructure, from the macroscopic one, which resolves the shape of Ω and the spatial variation of the applied field H_{ext}.

Consider a sequence (family) $\varepsilon \to 0$, and the corresponding fields v_ε, m_ε, and ψ_ε. Since the discrete phase variable p can be minimized out locally, we do not explicitly consider it in this discussion. We instead keep the potential of the demagnetization field ψ_ε explicit, since its treatment is subtle. For the macroscopic problem, ψ_ε is defined as the solution of (2.4) with zero boundary data at infinity, i.e., such that $\nabla\psi_\varepsilon$ is the $L^2(\mathbb{R}^2;\mathbb{R}^2)$-projection of m_ε onto gradient fields. Clearly the sequence m_ε is bounded in $L^\infty(\mathbb{R}^2;\mathbb{R}^2)$, hence it has a subsequence which converges weakly-* in $L^\infty(\mathbb{R}^2;\mathbb{R}^2)$ to some limit m_0. If the energy is bounded along the sequence, then ∇u_ε and $\nabla\psi_\varepsilon$ are also bounded in L^2, and hence - upon taking a further subsequence - have weak limits (in $L^2(\Omega;\mathbb{R}^2)$ and $L^2(\mathbb{R}^2;\mathbb{R}^2)$, respectively), call them v_0, ψ_0. Those limits are the fields corresponding to the macroscopic problem. Taking the weak limit of (2.4) we see that $\Delta\psi_0 = \operatorname{div} m_0$ (distributionally).

The key point is to understand which variational problem permits to determine v_0, m_0 (and ψ_0) without computing v_ε, m_ε (and ψ_ε) first. While a precise derivation of a homogenization result for the model considered here is still missing, knowledge obtained for many related problems motivate a very natural expectation. We expect a macroscopic variational problem of the form

$$\int_\Omega W^{\text{eff}}(m_0 \circ v_0, \nabla v_0)dx + \int_{\mathbb{R}^2} \frac{M_s^2}{2\mu_0}|\nabla\psi_0|^2 - \frac{M_s}{\mu_0} H_{\text{ext}} \cdot m_0 \, dy \tag{3.1}$$

plus appropriate boundary data on v_0. Here W^{eff} would be an effective energy density, which should be determined solving a microscopic cell problem. Notice that the integral of $H_{\text{ext}} \cdot m_\varepsilon$, being linear, converges to the integral of $H_{\text{ext}} \cdot m_0$; in general however $\lim \int |\nabla\psi_\varepsilon|^2 \geq \int |\nabla\psi_0|^2$.

For convex problems it is known that the only length scale entering the cell problem is that of the microstructure, and hence W^{eff} can be determined by solving cell problems of the size of the period of the microstructure. For nonconvex problems, such as the one considered here, additional length scales

can be spontaneously generated by the solution, and one needs to include the possibility for solutions to be periodic on an (arbitrary) integer multiple of the lengthscale of the microstructure, see [5, 28], or [6, Chap. 14]. An additional source of nonconvexity is the composition of m_0 with v_0, which however on the microscale (and for smooth v_0) is merely an affine change of variables.

For any material point $z \in \Omega$ in the macroscopic problem, we need to solve a microscopic problem for given macroscopic deformation gradient $F_0 = \nabla v_0(z)$, average magnetization $M_0 = m_0(z)$, and average demagnetization field $H_0 = \nabla \psi_0(z)$ (these quantities are treated as parameters, not as functions, in the discussion of the local problem). We consider a cell problem on the domain $(0,k)^2$, where $k \in \mathbb{N}$ represents the ratio between the length scale on which the microscopic solution is periodic, and the one on which the microstructure is periodic; one should take the infimum over all k, or, equivalently, the lim inf as $k \to \infty$. [In practice, for any fixed k in the next sections it will be convenient to rescale to the fixed domain $(0,1)^2$, and let the microstructure have a scale $1/k$; in the numerical simulations we shall only consider $k = 1$ or 2]. A case where $k = 1$ seems to be sufficient is illustrated in Figure 4, a case where for small applied external magnetic field it is not sufficient to consider only $k = 1$ is illustrated in Figure 13. On this domain, we seek the microscopic correctors to v_0, ψ_0, m_0. Precisely, we seek

$$v : (0,k)^2 \to \mathbb{R}^2 \,, \quad m : v((0,k)^2) \to \mathbb{R}^2 \,, \quad \psi : v((0,k)^2) \to \mathbb{R} \,.$$

The deformation field v should obey affine-periodic boundary conditions, where the affine part has a gradient given by the macroscopic deformation gradient F_0. This means that

$$v(x + ke_i) = v(x) + F_0 k e_i \qquad \text{for } x, x + ke_i \in \partial(0,k)^2 \,, \;\; i = 1,2 \,. \tag{3.2}$$

The magnetization should have average M_0, and obey the kinematic constraint. We require

$$|m|(y) = \begin{cases} 1 & \text{if } y \in \{v(\omega + \mathbb{Z}^2)\} \,, \\ 0 & \text{otherwise,} \end{cases} \tag{3.3}$$

and

$$\frac{1}{k^2} \int_{(0,k)^2} m(y)\, dy = M_0 \,. \tag{3.4}$$

The latter condition will be enforced through a Lagrange multiplier.

For the demagnetization potential, one natural option would be to define it as the solution ψ' to (2.4) which obeys affine-periodic boundary conditions:

$$\psi'(v(x + ke_i)) = \psi'(v(x)) + H_0 k e_i \qquad \text{for } x, x + ke_i \in \partial(0,k)^2 \,, \;\; i = 1,2 \,.$$

The full demagnetization field would then be $\nabla\psi'$, and the demagnetization energy would be its L^2 norm (with the appropriate dimensional factor). This would be consistent with the treatment of polarization fields in [43, 34, 26].

We instead prefer to define the field ψ as the solution of (2.4) which obeys periodic boundary conditions,

$$\psi(v(x+ke_i)) = \psi(v(x)) \qquad \text{for } x, x+ke_i \in \partial(0,k)^2\,,\ \ i=1,2\,.$$

This choice turns out to be more convenient, for a reason we now explain. We first observe that, since $\Delta\psi = \Delta\psi'$, one has $\psi'(y) = \psi(y) + H_0 \cdot y$ (up to an irrelevant additive constant). Therefore the full demagnetization energy decouples into

$$\int_{(0,k)^2} |\nabla\psi'|^2\,dy = \int_{(0,k)^2} |\nabla\psi + H_0|^2\,dy = \int_{(0,k)^2} |\nabla\psi|^2 + |H_0|^2\,dy\,, \qquad (3.5)$$

since by the periodicity of ψ the mixed product $2\nabla\psi \cdot H_0$ averages to zero on $(0,k)^2$. This decoupling is instrumental in separating the macroscopic part of the demagnetization energy $|H_0|^2 = |\nabla\psi_0|^2$, which we have already included in (3.1), from the microscopic one, $|\nabla\psi|^2$, which needs to be included in the cell problem. The advantage using ψ instead of ψ' is that the cell problem does not depend on the macroscopic H_0, but only on the macroscopic average magnetization M_0. The macroscopic demagnetization field H_0, which is determined from M_0 solving Laplace's equation on the macroscopic domain, only enters the macroscopic problem (3.1).

Finally, it remains to enforce the condition (3.4) on the magnetization. This is done via a Lagrange multiplier, which - being the variable conjugate to a magnetization - is naturally interpreted as an effective applied magnetic field, and is denoted by $h_{\rm ext}$. This field is *not*, however, to be identified with the magnetic field applied on the entire experimental probe: it is instead the effective field applied on the cell problem, which includes contributions from the rest of the sample. The microscopic problem in the upscaled domain $(0,k)^2$ therefore takes the form

$$\begin{aligned} E^{\rm micro}(F_0, h_{\rm ext}) \;=\; & \frac{1}{k^2}\inf\Bigg\{ E^{\rm elast}_{\rm matr}[v] + E_{\rm demag}[v,m] + \\ & \min_p \left[E^{\rm elast}_{\rm part}[v,p] + E_{\rm anis}[v,m,p]\right] - \frac{M_s}{\mu_0}\int_{(0,k)^2} h_{\rm ext}\cdot m \Bigg\}\,, \end{aligned}$$

where v and m are subject to (3.2) and (3.3). We stress that the final term coincides with $E_{\rm ext}$, after replacing the Lagrange multiplier $h_{\rm ext}$ for the external field $H_{\rm ext}$. At fixed F_0, the energy $E^{\rm micro}$ is a concave function of $h_{\rm ext}$,

being the infimum of a family of affine functions. The microscopic potential entering (3.1) can then be obtained by duality,

$$W^{\text{eff}}(F_0, M_0) = \sup_{h_{\text{ext}} \in \mathbb{R}^2} \left\{ \frac{M_s}{\mu_0} h_{\text{ext}} \cdot M_0 + E^{\text{micro}}[F_0, h_{\text{ext}}] \right\} . \tag{3.6}$$

To illustrate the significance of this decoupling, we discuss a case where a simple geometry permits to solve the macroscopic problem (3.1) analytically, namely, the case that Ω is a circle of radius R (similar arguments would work for the case of ellipses and ellipsoids, a fact already known to Maxwell [25], see [32]). It is known that application of a uniform magnetic field, say $H_{\text{ext}} = \bar{h} \in \mathbb{R}^2$, to a paramagnetic circle (or ellipse) results in a constant magnetization $m_0 = M_0 \in \mathbb{R}^2$. Equivalently, a uniformly magnetized sphere (circle, ellipse, ellipsoid) generates a uniform demagnetization field in its interior. Therefore the problem (3.1) has a stationary point with uniform m_0 and ∇v_0. The demagnetization field can also be computed analytically, and results in

$$\psi_0(x) = \begin{cases} \bar{m} x_1/2 & \text{if } |x| < R\,, \\ \bar{m} x_1 R^2/(2|x|^2) & \text{else,} \end{cases}$$

where for notational simplicity we assumed $M_0 = \bar{m} e_1$. The demagnetization energy can be computed explicitly, and the macroscopic problem (3.1) reduces to

$$E_{\text{macro}} = \pi R^2 W^{\text{eff}}(M_0, \bar{F}) + \frac{M_s^2}{2\mu_0} \frac{\pi R^2 |M_0|^2}{2} - \frac{M_s}{\mu_0} \pi R^2 H_{\text{ext}} \cdot M_0\,. \tag{3.7}$$

Minimizing in M_0 gives

$$\nabla_{M_0} W^{\text{eff}}(M_0, \bar{F}) + \frac{M_s^2}{2\mu_0} M_0 - \frac{M_s}{\mu_0} H_{\text{ext}} = 0\,.$$

In turn, from (3.6) we get

$$\nabla_{M_0} W^{\text{eff}}(M_0, \bar{F}) = \frac{M_s}{\mu_0} h_{\text{ext}}\,.$$

Hence the effective field acting on the microscopic problem is related to the external field, in this particular geometry, by

$$h_{\text{ext}} = H_{\text{ext}} - \frac{M_s}{2} M_0\,, \tag{3.8}$$

the factor $1/2$ being the demagnetization factor of the circle. In the case of an infinite slab (a domain of the kind $(0,1) \times \mathbb{R}$), the factor would be

0 for tangential fields, and 1 for normal fields. The same computation can be done for ellipses. In practice, if the reference configuration is a circle, under application of a magnetic field the MSM composite will deform to an ellipse, with eccentricity of a few percent. This results in a correction of a few percent to the demagnetization factor (which is 1/2 for the circle, in (3.8)); for simplicity we shall ignore this difference in the illustrative example in Section 6.3.

4 Rigid particles and linear elastic response

We are interested in the case where the active particles are small, and significantly harder than the polymer matrix; we can therefore assume their elastic deformation to be affine. The deformation gradient is then determined by energy minimization, and not constrained to coincide with the spontaneous strain. Let ω be the union of disjoint sets ω_i for $i = 1, \dots, N$ representing the particles. Furthermore, we assume them to be single crystals, which magnetically behave as single domains. Precisely, we assume that on each ω_i the crystal orientation Q, the deformation gradient ∇v, and the phase index p are constant, and let Q_i, F_i, p_i denote the corresponding values; we assume that on each $v(\omega_i)$ the magnetization m is constant, and let m_i denote its value. Since we are working in a linearized setting, we assume that the deformation v is close enough to the identity and thus injective.

We use linear elasticity, both for the matrix and the particles. Note, however, that we only linearize the deformation, not the lattice rotations $Q(x)$. In particular, we set $u(x) = v(x) - x$, and consider the quadratic elastic energy density for the polymer matrix

$$W_{\mathrm{matr}}(\nabla v) = W_{\mathrm{matr}}(\mathrm{Id} + \nabla u) \simeq W^{\mathrm{lin}}_{\mathrm{matr}}(\varepsilon(\nabla u))\,, \qquad \varepsilon(G) = \frac{1}{2}(G + G^T)\,.$$

Here $W^{\mathrm{lin}}_{\mathrm{matr}}$ is a quadratic form on symmetric 2×2 matrices, which can in the usual way be written in terms of the elasticity tensor C_{matr} [8]. We treat the polymer as an isotropic material, and write

$$W^{\mathrm{lin}}_{\mathrm{matr}}(\varepsilon) = \frac{1}{2} C_{\mathrm{matr}}\varepsilon : \varepsilon = \frac{1}{2}\lambda(\mathrm{Tr}\,\varepsilon)^2 + \mu|\varepsilon|^2\,.$$

The corresponding energy is

$$E^{\mathrm{lin}}_{\mathrm{matr}}[u] = \int_{\Omega\setminus\omega} W^{\mathrm{lin}}_{\mathrm{matr}}(\varepsilon(\nabla u))\,dx\,.$$

Notice that the displacement u has to satisfy the boundary condition

$$u(x + e_i) = u(x) + G_0 e_i \qquad \text{for } x, x + e_i \in \partial\Omega\,,\ \ i = 1, 2\,,$$

where $G_0 = F_0 - \mathrm{Id}$ is the macroscopic displacement gradient corresponding to the linear part of the cell deformation. Analogously, in the MSM particles for small strains F we have

$$W_{\mathrm{part}}(\mathrm{Id} + G, p) \simeq W^{\mathrm{lin}}_{\mathrm{part}}(\varepsilon(G) - \varepsilon_p)\,,$$

where the phase-dependent eigenstrains are as given in (2.2), and

$$W^{\mathrm{lin}}_{\mathrm{part}}(\varepsilon) = \frac{1}{2} C_{\mathrm{part}}\varepsilon : \varepsilon = \frac{1}{2} C_{11}(\mathrm{Tr}\,\varepsilon)^2 + (C_{12} - C_{11})\varepsilon_{11}\varepsilon_{22} + 2C_{44}\varepsilon_{12}^2\,.$$

Here C_{11}, C_{12} and C_{44} are the elastic constants in the elasticity tensor for the particles C_{part} under the assumption of cubic symmetry. Since we consider elastic deformations which are affine in each particle, we have

$$u(x) = G_i(x - x_i) + b_i \quad \text{for } x \in \omega_i\,.$$

Here $G_i = F_i - \mathrm{Id} \in \mathbb{R}^{2\times 2}$ is the displacement gradient in each particle, x_i the center of mass of the particle, and $b_i \in \mathbb{R}^2$ a shift.

The elastic energy of the particles from (2.1) can be written as

$$W_{\mathrm{part}}(FQ, p) = W_{\mathrm{part}}(Q^T FQ, p) = W_{\mathrm{part}}(\mathrm{Id} + Q^T(F - \mathrm{Id})Q, p)\,,$$

and expanding to leading order we obtain

$$E^{\mathrm{elast}}_{\mathrm{part}}[(G_i)_i, (p_i)_i] = \sum_{i=1}^{N} |\omega_i| W^{\mathrm{lin}}_{\mathrm{part}}\left(Q_i^T \varepsilon(G_i) Q_i - \varepsilon_{p_i}\right)\,.$$

As already discussed, we assume a uniform magnetization inside each particle,

$$m(y) = \begin{cases} m_i & \text{if } y \in v(\omega_i)\,, \\ 0 & \text{else.} \end{cases}$$

The interaction with the effective field can be written as

$$\begin{aligned} E_{\mathrm{ext}}[(G_i)_i, (m_i)_i] &= -\frac{M_s}{\mu_0} \int_{\mathbb{R}^2} h_{\mathrm{ext}} \cdot m \, dy \\ &= -\frac{M_s}{\mu_0} \sum_{i=1}^{N} |\det(\mathrm{Id} + G_i)|\, |\omega_i| h_{\mathrm{ext}} \cdot m_i\,. \end{aligned}$$

The computation of the demagnetization energy requires the solution of a Poisson problem, as specified in (2.4). Finally, the anisotropy term reduces to

$$E_{\mathrm{anis}}[(G_i)_i, (b_i)_i, (m_i)_i, (p_i)_i] = K_u \sum_i |\det(\mathrm{Id} + G_i)|\, |\omega_i| \varphi_{p_i}((R_i Q_i)^T m_i)\,.$$

Here R_i is obtained by the linearization of (2.5), namely,

$$R_i \approx \mathrm{Id} + \frac{1}{2}(G_i - G_i^T)\,.$$

The exchange energy is identically zero in this reduction of the model.

Material parameters and units. We use MKSA, and measure energy densities in $\mathrm{M\,Pa} = 10^6\ \mathrm{J/\ m^3}$. Length is considered to be dimensionless, or equivalently measured in fractions of the side length of the unit box $(0,1)^2$. This way we obtain directly energy densities that can be scaled to any macroscopic volume. The effective field h_{ext} is measured in Tesla; the practically used fields are of the order of 0.5 to 1 T [22, 38]. The constant entering E_{ext} is $\frac{M_s}{\mu_0} \simeq 0.50 \frac{\mathrm{M\,Pa}}{\mathrm{T}}$, where we used typical measured values for NiMnGa [22]. Correspondingly, the constant entering E_{demag} is expressed in terms of the first one via $\frac{M_s^2}{\mu_0} = \mu_0 \left(\frac{M_s}{\mu_0}\right)^2$, where $\mu_0 = \frac{4\pi}{10} \frac{\mathrm{T}^2}{\mathrm{M\,Pa}}$ (in practice, $M_s^2/\mu_0 \simeq 0.31\ \mathrm{M\,Pa}$). The anisotropy coefficient is approximately $K_u \simeq 0.13\ \mathrm{M\,Pa}$ [29, 38]. For the spontaneous strain in NiMnGa we take $\varepsilon_0 \sim 0.058$ and the elastic constants in NiMnGa are $C_{11} = 160\ \mathrm{G\,Pa}$, $C_{44} = 40\ \mathrm{G\,Pa}$, $C_{11} - C_{12} = 4\ \mathrm{G\,Pa}$ [37, 12] (see also [33]). The elastic modulus of the polymer matrix depends strongly on the type of polymer, typical values are of the order of a few $\mathrm{G\,Pa}$ [21]. We take $\lambda \sim 50\ \mathrm{G\,Pa}$, $\mu \sim 2\ \mathrm{G\,Pa}$, which are representative for epoxy and in what follows we fix the ratio between μ and λ.

5 Numerical Simulation

In this section we outline how we discretize the global energy and how we compute discrete minimizers numerically. The degrees of freedom in the simplified model derived in Section 4 are the linear part G_0 of the macroscopic deformation gradient, the elastic displacement u on the polymer matrix $\Omega \setminus \omega$, and for each particle i the displacement gradient G_i, the translation b_i acting on it, its phase parameter p_i, and its magnetization m_i. The only remaining continuous degree of freedom in our model is the displacement u. Besides that, we have to evaluate the magnetic potential ψ appearing in the demagnetization energy. All other quantities are discrete matrices, vectors, or scalar quantities. To eliminate the two continuous fields, we proceed as follows.

Discretization of the domain. First we discretize the domain and represent $\partial\Omega$ and $\partial\omega_i$ by polygons. In the applications below, we always consider identical shapes for the particles ω_i and correspondingly identical

polygonal approximations ω_i^h. Here, h denotes the maximal distance between two consecutive points on the polygonal outline of a particle. In addition the distance between discretization nodes on $\partial\Omega$ is ensured to be bounded by h as well.

Polymer elasticity. For given G_i and b_i, and for a given macroscopic displacement gradient G_0, the displacement u is the solution of the linear elastic problem

$$\begin{aligned} \operatorname{div} C_{\mathrm{matr}}\varepsilon(\nabla u) &= 0\,, && \text{in } \Omega\setminus\omega\,,\\ u &= G_i(\cdot - x_i) + b_i\,, && \text{on } \partial\omega_i \quad \text{for } i = 1,\dots,N\,,\\ u(\cdot + e_i) &= u + G_0 e_i\,, && \text{on } \partial\Omega\,. \end{aligned}$$

For the discretization a collocation boundary element method [2, 10] with affine ansatz functions is applied. We use a direct approach based on Greens formula that relates the values of the displacement u and the normal stress $C_{\mathrm{matr}}\varepsilon(\nabla u)\nu$ on the boundary by an integral equation. Here, ν is the outer normal on $\partial(\Omega\setminus\omega)$. As actual degrees of freedom we consider these boundary values at vertices on $\partial\Omega$ and on $\partial\omega_i^h$.

Due to periodicity, only one half of the displacement and stress values on the boundary of Ω are actual degrees of freedom. In fact, one has to pay close attention to the handling of the stress values in the corners: We approximate the normal stress by piecewise affine, continuous functions along the faces of Ω. In the corners continuity is required for the full stress matrix. As the faces of Ω are straight, this is equivalent to requiring the normal-stress to be (one-dimensionally) periodic along those faces.

Given the numerical solution in terms of these degrees of freedom, the elastic energy on the polymer matrix can be evaluated using the discrete analog of the following continuous integral representation:

$$\begin{aligned} E_{\mathrm{elast}}^{\mathrm{matr}}[v] &= \int_{\Omega\setminus\omega} \frac{1}{2} C_{\mathrm{matr}}\varepsilon : \varepsilon \, dx = \int_{\Omega\setminus\omega} \frac{1}{2} C_{\mathrm{matr}}\varepsilon : \nabla u \, dx\\ &= -\frac{1}{2}\int_{\Omega\setminus\omega} \operatorname{div} C_{\mathrm{matr}}\varepsilon \cdot u \, dx + \frac{1}{2}\int_{\partial\Omega\cup\partial\omega} (C_{\mathrm{matr}}\varepsilon\nu)\cdot u \, ds_x\\ &= -\sum_{i=1,2}\frac{1}{2}\int_{E_i} (C_{\mathrm{matr}}\varepsilon\nu)\cdot(G_0 e_i)\, ds_x + \frac{1}{2}\int_{\partial\omega} (C_{\mathrm{matr}}\varepsilon\nu)\cdot u \, ds_x\,. \end{aligned}$$

Here, ds_x denotes the length element in the reference configuration. Due to the affine periodicity of u, we only need evaluate the difference of u along the two faces $E_i = \{x | x, x + e_i \in \partial\Omega\}$ of the outer boundary.

Demagnetization. For given magnetization $(m_i)_i$ and deformation $v = \mathrm{Id} + u$ on the polymer matrix the potential ψ (required for the evaluation of

the demagnetization energy) is given as the solution of (2.4), i.e.,

$$\begin{aligned} \Delta\psi &= 0\,, && \text{in } v(\Omega \setminus \partial\omega)\,,\\ [\nabla\psi \cdot \nu] &= m \cdot \nu\,, && \text{on } v(\partial\omega)\,,\\ \psi(\cdot + F_0\, e_i) &= \psi\,, && \text{on } \partial v(\Omega)\,, \end{aligned}$$

where ν is the outer normal on the deformed particle boundary $v(\partial\omega_i)$, m the magnetization of the particle, and $[\cdot]$ is the corresponding jump operator on this set. We fix the arbitrary additive constant by setting $\int_{\partial\omega} \psi = 0$. For the numerical solution, we again apply a collocation boundary element method with piecewise constant ansatz functions. As above, the evaluation of the energy can be based solely on the computation of boundary integrals. Indeed, we obtain

$$\begin{aligned} E_{\mathrm{demag}}[v,m] =& \frac{M_s^2}{\mu_0} \int_{v(\Omega)} \frac{1}{2} |H_d|^2 \, dy = \frac{M_s^2}{\mu_0} \int_{v(\Omega)} \frac{1}{2} |\nabla\psi|^2 \, dy \\ =& \frac{1}{2} \frac{M_s^2}{\mu_0} \left(- \int_{v(\Omega\setminus\omega)} \Delta\psi\psi \, dy + \int_{v(\partial\Omega)} (\nabla\psi \cdot \nu)\psi \, ds_y \right. \\ & \qquad \left. + \int_{v(\partial\omega)} [\nabla\psi \cdot \nu]\psi \, ds_y \right) \\ =& \frac{1}{2} \frac{M_s^2}{\mu_0} \int_{v(\partial\omega)} (m \cdot \nu)\psi \, ds_y \,, \end{aligned}$$

where ds_y denotes the length element in the deformed configuration.

Numerical Relaxation. So far we have discussed how to compute numerical approximations for the elastic displacement u and the magnetic potential ψ. Now, we confine to the following set of degrees of freedom $(G_0, (G_i)_i, (m_i)_i, (p_i)_i) \in \mathbb{R}^{4+4N+2N+N}$ and suppose $u[G_0, (G_i)_i]$ to be the minimizing displacement in the polymer matrix for given linear component G_0 of the global cell displacement and given distinct particle displacements G_i. This allows us to redefine the global energy, now solely depending on the above set of degrees of freedom. In fact, for each evaluation of the energy we have to solve a linear elastic problem in the polymer phase and a demagnetization problem as described above. For the minimization of the energy over the remaining set of parameters in $\mathbb{R}^{7N+4}$ we apply a gradient descent method. The gradient is calculated using central difference quotients with a step size δ. The control of the time step size τ in the actual descent algorithm is based on the Armijo rule. The spatial step size δ is adjusted to the temporal step size τ if indicated by the step size control.

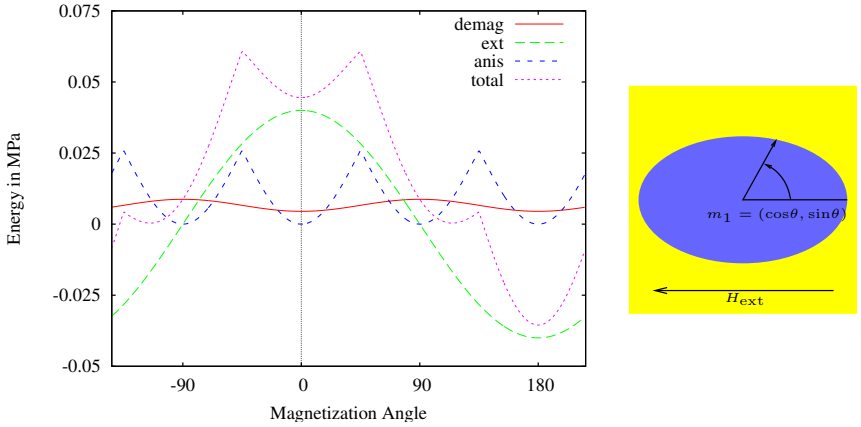

FIGURE 2: Energy landscape as a function of m, for fixed deformation. We consider one elliptical, horizontally (i.e., along e_1) elongated particle, prescribe zero elastic displacement $G_0 = G_1 = 0$, and prescribe the magnetization, $m_1 = (\cos\theta, \sin\theta)$. The figure shows E_{demag} (red, full), E_{ext} (green, long-dashed) E_{anis} (blue, short-dashed), and their sum (magenta, dotted), as functions of θ. The global minimum is achieved at $\theta = 180°$, the figure is 360°-periodic, the figure plots one period. Here, we take a relatively small external field $H_{\text{ext}} = 0.1$ T in direction $-e_1$, volume fraction 40%, aspectratio 1.6:1, and the other parameters as in Section 4.

Validation. We first compute the different energy terms fixing all variables. In Figure 2 we report the energy as a function of magnetization direction, with no elastic deformation of the matrix. The switching between the two phases is apparent from the behavior of the anisotropy energy.

In order to test the correct implementation of the affine-periodic boundary conditions we compared results for a single particle in a square box, with four particles in a box four times larger (which, after periodic continuation, amounts to exactly the same global configuration). For a circular particle of radius 0.4, in a box of side length 1, discretized with 32 points, we compute the spontaneous strain of 0.0735537 and the energy per unit volume of 2.91812 M Pa. The computation with four particles gave a strain of 0.0735533 and an energy density of 2.91845 M Pa, which is the same within numerical accuracy.

To check dependence on the grid size, we computed the energy diagrams for different number of discretization points, see Figure 3. For a fixed strain, the energy converges quadratically in the grid size, as can be seen from the estimated order of convergence $\text{eoc}(E)(N) := \log(\frac{E_{N/4}-E_{N_{\max}}}{E_N-E_{N_{\max}}})/\log(4)$ reported in Table 1. The convergence in the position of the minimum, i.e., on the spontaneous strain is even faster, see Table 2.

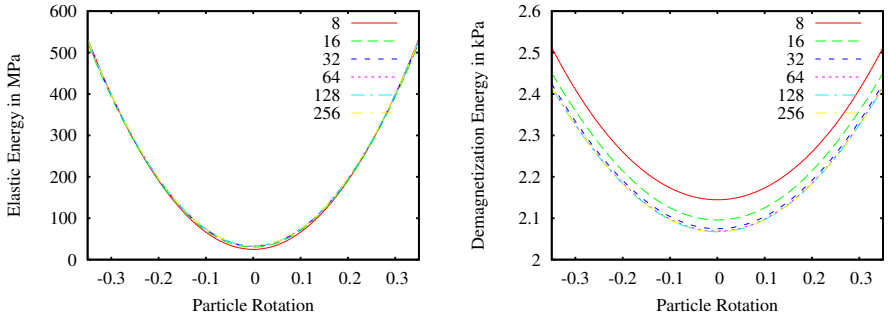

(a) (b)

FIGURE 3: Elastic energy of polymer (a) and demagnetization energy (b) , as functions of a small particle rotation. In the same setting as in Figure 2, we now fix m and change the skew-symmetric part of G_1. The figure shows the graph of energy over rotation $((G_1)_{12} - (G_1)_{21})/2$ for a number of sequentially refined discretizations. The symmetric part is kept fixed at the value $G_1 = (-0.04, 0.04)$.

N	$\mathrm{eoc}(E^{\mathrm{elast}}_{\mathrm{matr}})$	$\mathrm{eoc}(E_{\mathrm{demag}})$	$\mathrm{eoc}(E)$	E in MPa
32	1.69	0.68	1.71	89.8175
128	2.13	1.99	2.12	91.3056
512	2.13	2.26	2.24	91.3850
1024				91.3888

TABLE 1: Estimated order of convergence for the energy components whose computation involves BEM. The configuration is the same as above, where the energy is evaluated in some deformed configuration (still significantly away from the minimum). The energy in the finest computation (that was used as a point of reference for the eoc) was 91.3888.

6 Results

For any given set of material parameters and geometry, and fixed external field, we compute the energy as a function of external field and macroscopic deformation, $E[F_0]$. The spontaneous deformation $\bar{F}_0$ is then determined as the matrix which minimizes $E[F_0]$; since the phase transition occurs at constant volume, the determinant of F_0 turns out to be always very close to unity. We report in the following the spontaneous deviatoric strain, i.e.,

$$(\lambda_2 - \lambda_1)(\bar{F}_0)\,,$$

$\lambda_i(F)$ being the ordered singular values of F (i.e., the eigenvalues of $(F^T F)^{1/2}$). In all deformation figures we plot first the reference configuration, corresponding to $u = 0$ and $F_0 = \mathrm{Id}$, and then the deformed one at the spontaneous macroscopic deformation, where $F_0 = \bar{F}_0$. For simplicity of illustration,

N	$\lambda_2 - \lambda_1$	min$E$
32	0.0197835	3.20766
64	0.0198949	3.21424
128	0.0198934	3.21583

TABLE 2: Convergence for the position and value of the minimum. We consider one circular particle of volume fraction 20%, $\mu = 2$ GPa and $H_{\text{ext}} = 1$ T. We compute the difference of the two eigenvalues of G_0 (which is diagonal due to the symmetry of the configuration).

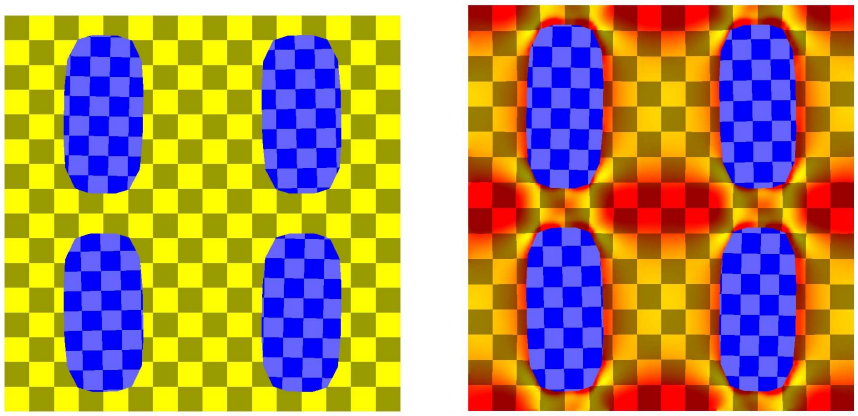

(a) (b)

FIGURE 4: Deformation of four (nearly) exactly oriented particles, with total volume fraction of 29.1%. (a): Reference configuration, (b): Deformed configuration. The macroscopic strain is 4.8%. In comparison, the maximal strain of NiMnGa single-crystals is 11.6%. The checkerboard pattern illustrates the elastic deformation (it is not related to a numerical mesh), the color coding represents the strain in the matrix visually (yellow=low strain, red=high strain; as strain measure we use the elastic energy density $W_{\text{matr}}^{\text{lin}}$, the scale ranges from 0 to 5 MPa). The checkerboard in the particle domain indicates the crystal orientation.

in the whole section we consider particles with lattice orientation along the orientation of the symmetry axis of their shape.

6.1 Four aligned vs. four misaligned particles

In Figure 4 we consider four particles with (almost) the same orientation, in the presence of an external field. Even with a rather small volume fraction the spontaneous strain is only one-half of the one of a single crystal. The stress in the polymer concentrates in the small regions between the particles.

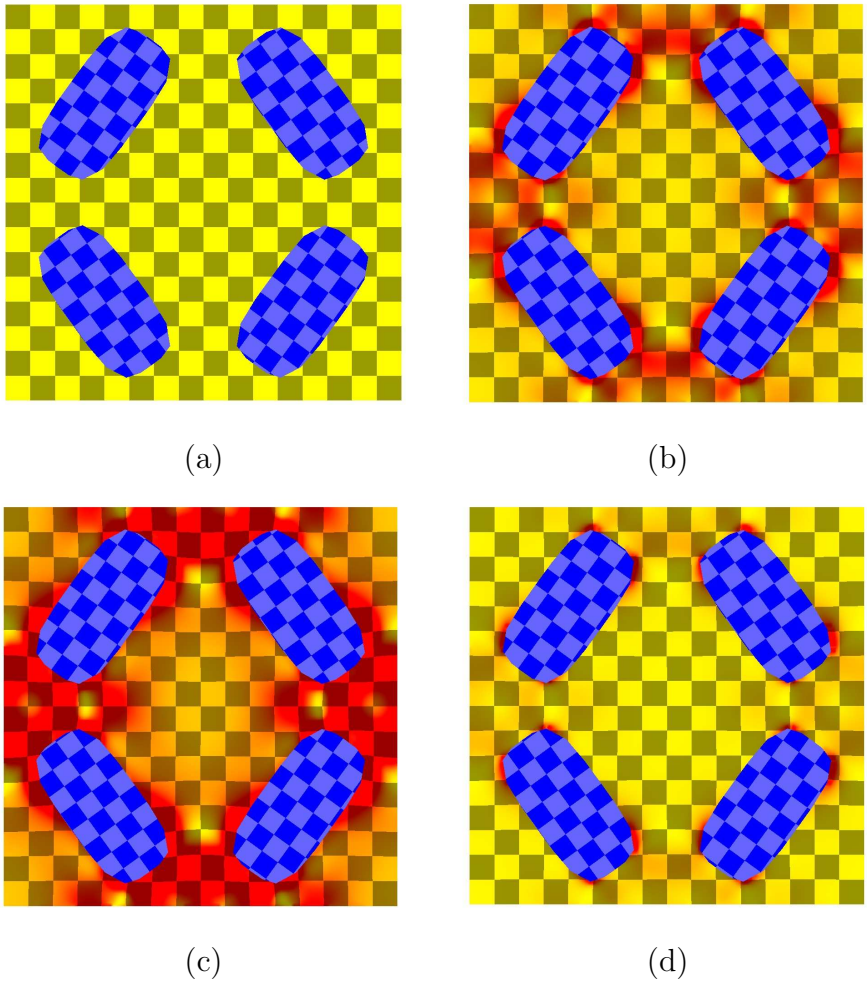

FIGURE 5: Deformation of four severely misoriented particles. (a): Reference configuration; (b): Deformed configuration. The macroscopic strain is 0.9%. On the bottom we show the same computation for a polymer that is softer (c) or harder (d) by a factor of 2, exhibiting a strain of 1.4% or 0.5% respectively.

The entire configuration is almost completely rotation-free.

If the orientation of the particles is instead very different, see Figure 5, then the macroscopic spontaneous strain, for exactly the same particles, sinks by a factor of 5. Each particle still transforms as in the previous case; the eigenstrains of the particles are

$$\varepsilon^{(i)} = Q_i \varepsilon_1 Q_i^T , \qquad Q_i = \begin{pmatrix} \cos\theta & \pm\sin\theta \\ \mp\sin\theta & \cos\theta \end{pmatrix} ,$$

where $\theta = 36°$. Here ε_1 was defined in (2.2). The (tensorial) average of these eigenstrain is $\langle \varepsilon^{(i)} \rangle = \cos\theta \varepsilon_1$, therefore it is about 20% smaller than

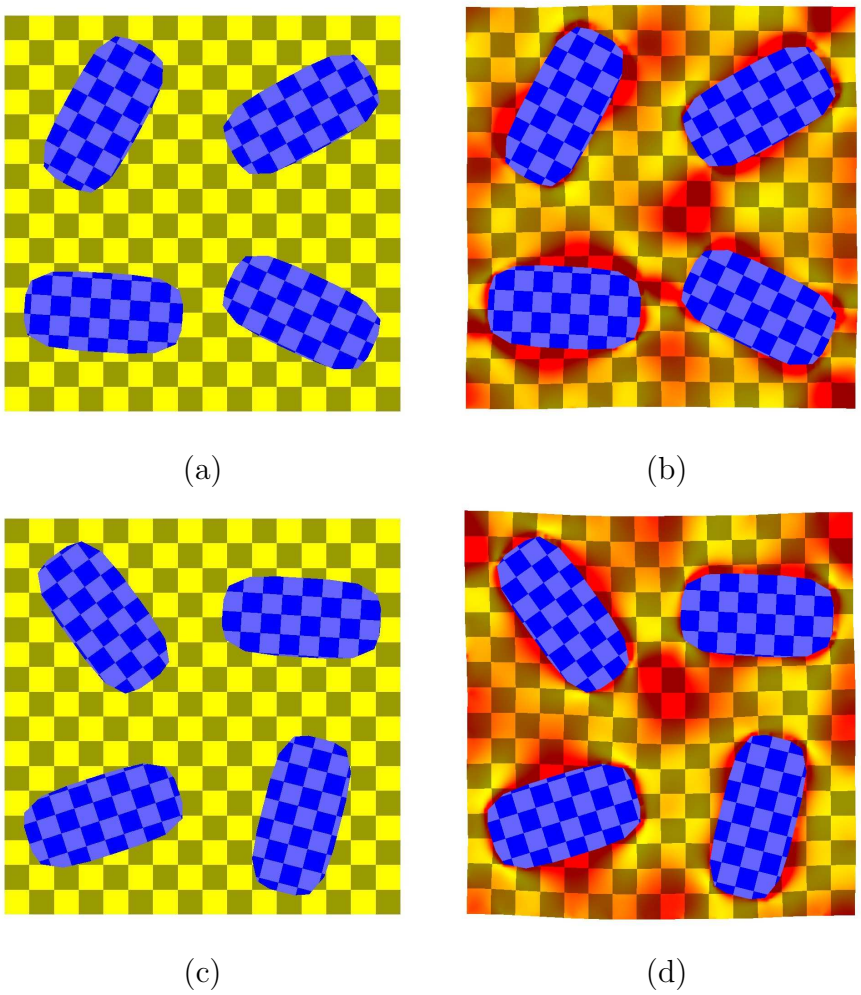

FIGURE 6: Two different random configurations. (a) and (c): Reference configuration; (b) and (d): Deformed configuration. The macroscopic strain is 2.8% in the first and 3.7% in the second case.

the one pertaining to the oriented configuration in Figure 4. The reduction in macroscopic deformation is, however, much larger. This is due to the fact that the eigenstrains are incompatible, and that this incompatibility has to be accommodated by the polymer. The resulting polymer deformation around each particle reduces the macroscopic effect of the eigenstrain, and indeed the polymer is almost completely under significant strain. If one considers softer polymers, then accommodation of strain is easier, and the spontaneous strain increases, as the lower part of the figure shows. For very soft polymers one can easily get large spontaneous shears, but the work output will be extremely small, see also the discussion below.

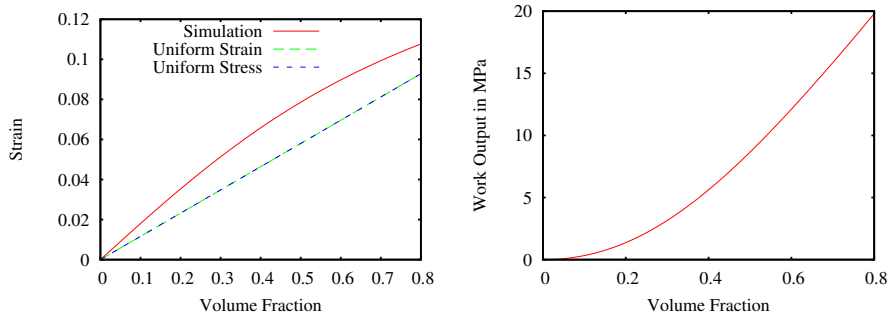

(a) (b)

FIGURE 7: Effect of volume fraction. For a particle with aspectratio 1, we change the volume. Parameters as above. (a): Resulting strain $(\lambda_2 - \lambda_1)(F_0)$ as a function of volume. (b): Work output, as a function of volume.

Finally, Figure 6 shows for comparison two different random distributions of the particles, which results in intermediate values of the spontaneous strain.

6.2 Systematic investigation of individual parameters

We now turn to a more systematic investigation of the effect of changing individual parameters. The quality of the material is determined in terms of the spontaneous strain, defined above, and the work output, defined as

$$\text{Work output } = (\text{Energy at } F_0 = \mathrm{Id}) - \big(\text{Energy at } F_0 = \bar{F}_0\big) \ .$$

All energies are evaluated per unit volume, and measured in $\mathrm{M\,Pa}$.

We start from the simplest parameter, namely, the volume fraction. Figure 7 shows the spontaneous strain and the work output for circular particles of different volume, and lattice rotations $Q_i = \mathrm{Id}$. We compare the numerical results with the two simple approximations used in the homogenization literature, namely, uniform strain and the uniform stress.

The uniform-strain model, in the present setting, amounts to the assumption that $G_i = \nabla u(x) = G_0$ for all i and all x. The elastic energy then takes the form

$$E_{\text{u.strain}}[G_0] = |\Omega \setminus \omega| W^{\text{lin}}_{\text{matr}}(G_0) + \sum_i |\omega_i| W^{\text{lin}}_{\text{part}}(Q_i^T G_0 Q_i - \varepsilon_{p_i}) \, . \qquad (6.1)$$

The geometry of the microstructure has completely disappeared from the picture. The coupling to the magnetic field is in turn – up to a very small influence of G_0 on the demagnetization energy – reduced to the value of p_i.

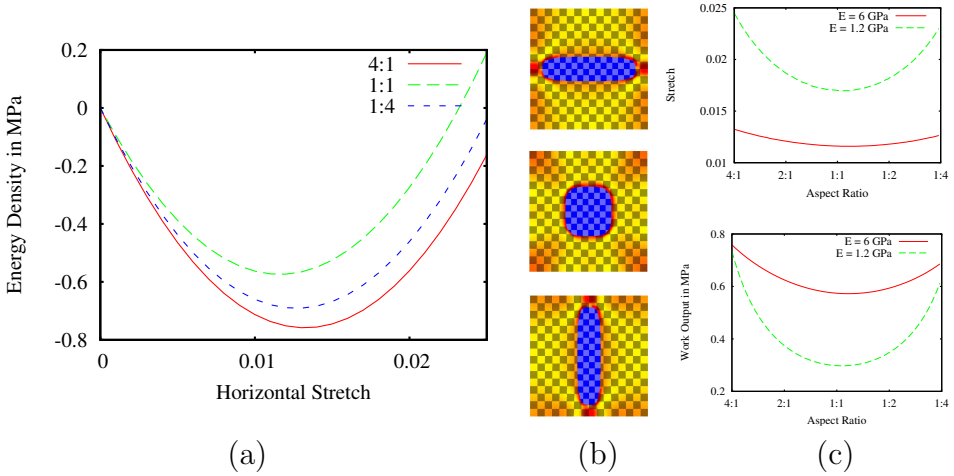

FIGURE 8: Effect of aspectratio. Particle and parameters as described above. (a): Energy as a function of strain, for different aspectratios. (b): Deformed configurations, for the same three values of the aspectratio. (c): Spontaneous stretch and work output as a function of aspectratio. Additionally, the green curves in (c) also plot the functions for a polymer that is five times softer than our standard configuration.

Therefore a simple minimization of the quadratic expression in (6.1) gives the optimal value for $F_0 = G_0 + \mathrm{Id}$.

In the uniform stress approximation one instead assumes the stress to be constant and equal to the macroscopic value, which is zero for the equilibrium state. Correspondingly, the deformation gradient vanishes in the matrix, and coincides with the spontaneous strain in the particles. The spontaneous macroscopic deformation gradient is

$$\bar{G}_0 = \sum_i |\omega_i| Q_i^T \varepsilon_{p_i} Q_i \,. \tag{6.2}$$

Variants of these approximations have been used in the literature on magnetoelastic composites, see, e.g., [7, 20]. Figure 7 shows that for the specific parameters used here the two approaches give the same result, which describes the increase in spontaneous strain with volume fraction in a qualitatively correct manner.

Next we consider the effect of the aspectratio of the particles, keeping the volume constant. In Figure 8 we show that the extreme values of the

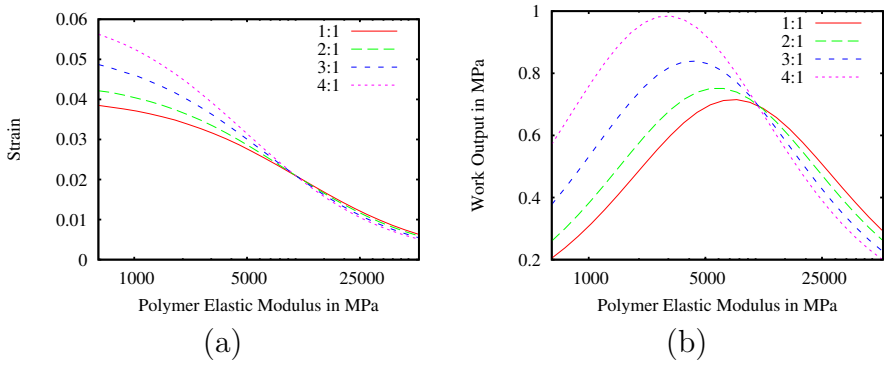

FIGURE 9: Effect of polymer elastic moduli. Volume fraction 15%, aspectratios 4:1, 3:1, 2:1, and 1:1, other parameters as above. (a): Strain as a function of polymer elastic modulus $E = \mu(3\lambda + 2\mu)/(\lambda + \mu)$. (b): Work output as a function of polymer elastic modulus (where $\nu = 0.48$, so that the ratio λ/μ remains constant). The scale for E is logarithmic.

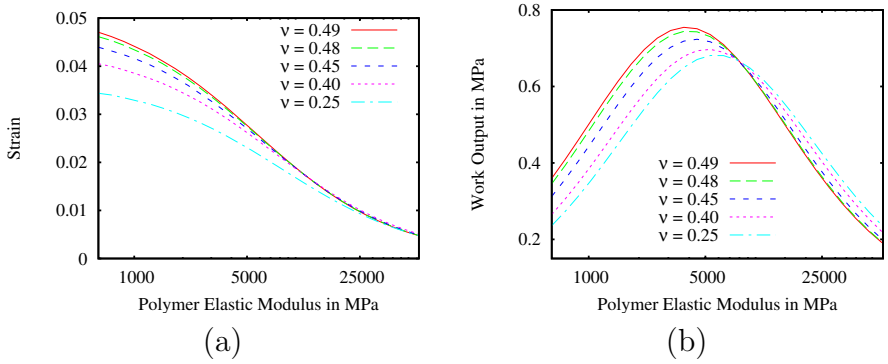

FIGURE 10: Effect of polymer elastic moduli. Volume fraction 15%, aspectratio 3:1, Poisson ratios 0.49, 0.48, 0.45, 0.4, and 0.25. (a): Strain as a function of polymer elastic modulus E. (b): Work output as a function of polymer elastic modulus, as in Figure 9.

aspectratio give both a higher work output, and a higher spontaneous strain.

Figure 9 illustrates the effect of the elastic modulus of the polymer. We first scale the Young modulus keeping the Poisson's ratio constant, which corresponds to multiplying λ and μ by the same factor. As expected, soft polymers lead to large spontaneous deformation, and small work output. These quantitative computations show that the maximum work output is achieved for polymers significantly softer than the particles, in particular for large aspectratio.

Figure 10 shows that varying Poisson's ratio does not have a major influence on those results.

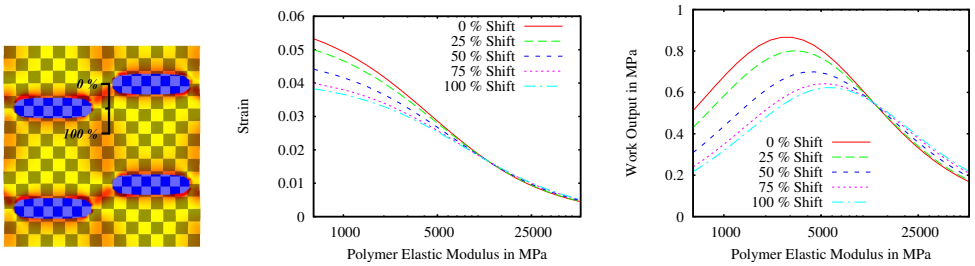

(a) (b) (c)

FIGURE 11: Effect of polymer shear modulus for oriented, non-aligned particles. Volume fraction 14%, aspectratio 4:1 with 4 particles in the unit box. We plot the effect of the polymer elasticity for different degrees of misalignment, where particles in one row are shifted with respect to particles in the other row; 100% signifies the maximal misalignment. (a): Configuration for 50% offset. (b): Strain as a function of polymer elastic modulus. (c): Work output as a function of polymer elastic modulus. Here the Poisson's ratio ν is kept constant, the scale for E is logarithmic.

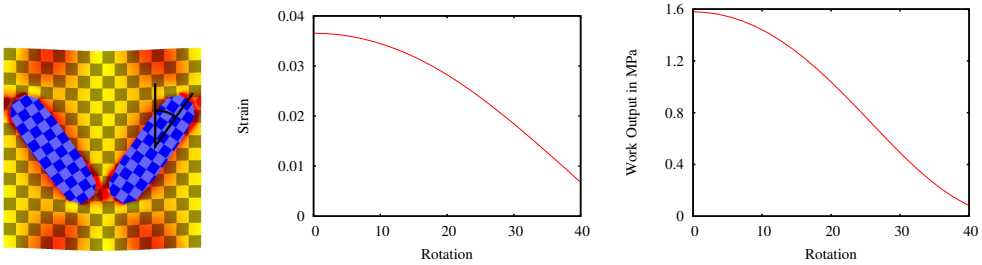

(a) (b) (c)

FIGURE 12: Effect of orientation. Two elongated particles. Volume fraction 22%, aspectratio 3:1. We vary the misorientation angle, i.e., the angle between the axis of the two particles. Other parameters as above. (a): Geometry. (b): Strain as a function of the angle between particle axis and e_2. (c): Work output.

We finally come back to the oriented particles of Figure 4, and consider the effect of loss of structure. First, we consider particles which still all have almost exactly the same orientation, but which are not aligned. We show in Figure 11 that even strongly misaligned, but oriented, particles lead to large spontaneous deformations.

In Figure 12 we consider the effect of orientation. The curves show the dramatic effect of particle orientation on both spontaneous shear and work output. We stress that capturing this geometric effect requires resolution of the elastic deformation of the polymer, and that both simple models mentioned above would not detect any effect of aspectratio, alignment and ori-

entation.

6.3 Role of the demagnetization field

We first observe that the effects discussed are almost totally the consequence of the phase transition, and that the deformation arising from the dipole-dipole magnetic force acting on the magnetized particles is negligible. In the configuration of Figure 5, for example, the rotation of the particles coming from the magnetic force is not more than 10^{-3} degrees (barely resolved by our numerics), and the contribution to the total strain is somewhat smaller. Even making the polymer 100 times softer, the strain arising from the magnetic force remains less than 10^{-3}. In the configuration of Figure 4 this effect vanishes completely by symmetry. This applies taking as a representative case $h_{\text{ext}} = 1$ T. In experiment one usually considers external fields H_{ext} of order 1 T, motivated by the effects such as metastable states, barriers, and disorder. In practice, for an applied field is $H_{\text{ext}} = 1$ T, the local effective field h_{ext} will be slightly different. In what follows, we argue that this difference is negligible in this parameter range.

The difference between the macroscopic and the microscopic field is expressed for a simple geometry in (3.8). At least for this case, it is easy to see that the difference is not very large. Indeed, since $|M_0|$ is less than or equal to the volume fraction of the active material, and $M_s \sim 0.6$ T, the term $M_s M_0/2$ is, with our material parameters and our typical volume fraction 0.15, of order 0.05 T. This is much smaller than the value of $H_{\text{ext}} = 1$ T. The correction becomes of course important for very weak applied fields (or in special geometries).

Let us make this analysis more precise with a quantitative computation on a circular domain Ω, for which the macroscopic demagnetization field can be computed analytically as discussed in Section 3. We consider a microstructure of aligned, elongated particles with a large volume fraction (to enhance M_0) and compare the case where all particles are magnetized in the same direction (which is favored by the interaction with the external field) with the case where neighboring particles are magnetized in opposite directions (which is favored by the macroscopic demagnetization energy), see Figure 13, which shows energy graphs of the different magnetization configurations for varying external field. The same figure also provides an example where the periodicity of the solution is a nontrivial multiple of the periodicity of the microstructure; we work therefore with four or sixteen periods in the unit cell.

If neighboring particles are magnetized in opposite directions (see (a) in Figure 13), the macroscopic magnetization m_0 vanishes, and the only con-

tribution to the demagnetization field is from the microscopic part. Quantitatively, it turns out to be 5.8 k Pa. If all particles are magnetized in the same direction (see (c) in Figure 13), then the macroscopic magnetization m_0 equals the microscopic one, times the volume fraction. The microscopic part of the demagnetization field contributes 12 k Pa, while we get a contribution from the macro-scale of 19 k Pa per unit volume (the entire contribution from the demagnetization field scales as volume). The interaction with the external field subtracts 250 k Pa per Tesla (since the volume fraction is about 50%). We conclude that the fully magnetized state (c) is energetically favourable over the fully demagnetized state (a) for applied fields larger than about 100 m T.

In fact, a full analysis of the four-period cell shows that in between these two situations there is another regime, where only one of the four particles in the computational cell is magnetized in the direction opposite to the external field (see (b) in Figure 13). All other states are never energetically optimal. An external magnetic field of less than 200 m T is sufficient to switch from oscillating to uniform magnetization of particles in this setting.

As we discussed in Section 3, increasing the size of the computational cell increases the number of possible states, and – since the problem considered here is not convex – in general one expects that energetically more convenient states are found that way. We display this exemplarily in the right-hand column of Figure 13, considering three of the $2^{16} - 2^4 = 65520$ new states arising in a cell with double side length. One has only a single particle directed against the field (f). This head-head configuration has a rather large microscopic demagnetization field, and turns out never to be optimal. Another has two particles, in a head-tail configuration, directed against the field (e) and is the obvious generalization to a higher period of the configuration (b) discussed above; this indeed turns out to have lower energy than all other considered states in some interval of applied fields (see Figure 13). A similar configuration of six particles in three lines (d) turns up between the states (a) and (b). Extension for even larger size of the computational cell are of course possible, but numerically they become exponentially more and more expensive.

6.4 Comparison with Ref. [24]

Our numerical results are in good qualitative agreement with analytical results obtained for ellipsoidal particles in the dilute limit [24]. At a quantitative level, however, some differences are apparent. In particular, the optimal value of the matrix elastic modulus we predict is at least an order of magnitude larger than the one predicted in [24] (compare Figure 9(b) with

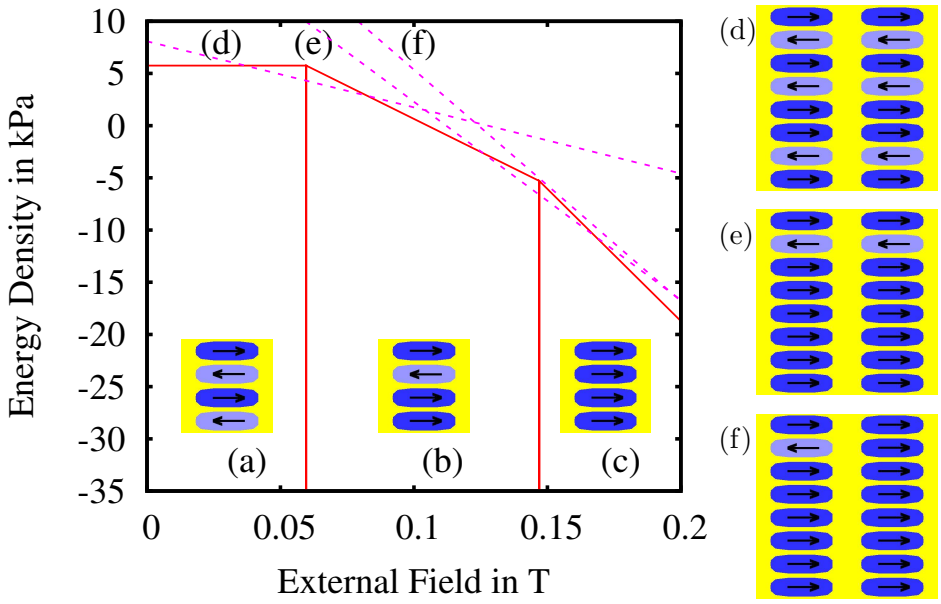

FIGURE 13: Effect of the macroscopic part of demagnetization, for a unit cell containing four identical elongated particles. The aspectratio of each particle is 7:2, the volume fraction 50%, the macroscopic demagnetization field for a circular macroscopic domain is included via (3.7). The graph shows the total energy as a function of the external magnetic field H_{ext} and the three microscopic magnetization patterns (a) – (c) in the unit cell which are optimal in a part of the considered range of H_{ext}. It is natural to expect that simulations with more particles in the computational cell will give a richer phase diagram: For example, in a computational cell four times as large, we additionally considered the states (d) – (f) displayed on the right-hand side of the total of 2^{16} possibilities for the magnetization of each particle. The state (f) has only one of the 16 particles directed against the magnetic field and turns out never to be optimal. The states (d) and (e) are additional ground states in intermediate ranges of the magnetic field between the patterns (a), (b) and (b), (c), respectively.

[24, Figure 7]). Among the many effects which contribute to this difference (dimensionality, volume fraction, validity of the dilute limit and of the constrained elasticity used in [24], etc.) we believe that the main discrepancy lies in the modeling of the particles. We have focused here on *small* particles, which are not only single crystalline, but also magnetically behave as monodomain. In [24] the particles are instead considered to be *large* (on the scale of the size of magnetic domains), and the overall behavior of any single particle is determined by averaging over all possible domain structures, without any nucleation barrier, and any energetic cost for domain boundaries. This renders the MSM particles effectively much softer, and makes it much easier for the polymer to inhibit the transformation: therefore one needs softer polymers in this model. An improved model should take care of the fact that

the two length scales may well be comparable, in particular since the size of domains in the MSM particles will be, in turn, influenced by the polymer, and can therefore only be determined a posteriori. If the possibility of multidomain structures in the particles is considered, and domain boundaries are penalized via the exchange energy, one will obtain scale-dependent results, which are expected to interpolate between the two mentioned extrema.

7 Conclusions

In summary, we presented a model to study the microstructure of composites of magnetic-shape-memory particles in a polymer matrix. We developed a numerical method to solve the model efficiently, in two dimensions and within a geometrically linear setting, on the basis of the boundary-element method. Our results underline the importance of orienting the particles in the composite, and show that alignment is instead a much less critical aspect. We recall that application of a magnetic field during solidification is a simple and known method to force orientation, but does not permit to control alignment. Furthermore, we have shown that a polymer somewhat softer than the particles gives the optimal work output, and that elongated particles have much better properties than circular ones.

Acknowledgements

This work was partially supported by Deutsche Forschungsgemeinschaft through the Schwerpunktprogramm 1095 *Analysis, Modeling and Simulation of Multiscale Problems*.

References

[1] F. Albertini et al., *Magnetoelastic effects and magnetic anisotropy in Ni_2MnGa polycrystals*, J. Appl. Phys. **89** (2001), 5614–5617.

[2] K. E. Atkinson, *The numerical solution of integral equations of the second kind*, Cambridge Univ. Press, 1997.

[3] G. Bertotti, *Hysteresis in magnetism*, Academic Press, 1998.

[4] K. Bhattacharya, *Microstructure of martensite: Why it forms and how it gives rise to the shape-memory effect*, Oxford University Press, 2003.

[5] A. Braides, *Homogenization of some almost periodic coercive functionals*, Rand. Accad. Naz. Sci. XL Mem. Mat. **9** (1985), 313–321.

[6] A. Braides and A. Defranceschi, *Homogenization of multiple integrals*, Claredon Press, Oxford, 1998.

[7] Y. Chen et al., *Effect of the elastic modulus of the matrix on magnetostrictive strain in composites*, Appl. Phys. Lett. **74** (1999), 1159–1161.

[8] P. G. Ciarlet, *Three dimensional elasticity*, Mathematical elasticity, vol. I, Elsevier, Amsterdam, 1997.

[9] D. Cioranescu and P. Donato, *An introduction to homogenization*, Oxford Univ. Press, Oxford, 1999.

[10] D. L. Clements and F. J. Rizzo, *A method for the numerical solution of boundary value problems governed by second-order elliptic systems*, J. Inst. Maths. Applics **22** (1978), 197–202.

[11] S. Conti, M. Lenz, and M. Rumpf, *Macroscopic behaviour of magnetic shape-memory polycrystals and polymer composites*, preprint (2006).

[12] L. Dai, J. Cullen, J. Cui, and M. Wuttig, *Anomalous behavior of the elastic constants in NiMnGa*, preprint (2005).

[13] A. DeSimone and R. D. James, *A theory of magnetostriction oriented towards applications*, J. Appl. Phys. **81** (1997), 5706–5708.

[14] ———, *A constrained theory of magnetoelasticity*, J. Mech. Phys. Solids **50** (2002), 283–320.

[15] X. Feng, D. N. Fang, and K. C. Hwang, *Closed-form solutions for piezomagnetic inhomogeneities embedded in a non-piezomagnetic matrix*, Eur. J. Mech. A **23** (2004), 1007–1019.

[16] J. Feuchtwanger et al., *Energy absorpion in Ni-Mn-Ga polymer composites*, J. Appl. Phys. **93** (2003), 8528–8530.

[17] ———, *Mechanical energy absorpion in Ni-Mn-Ga polymer composites*, J. Magn. Mag. Mat. **272-276** (2004), 2038–2039.

[18] A. Hubert and R. Schäfer, *Magnetic domains*, Springer, Berlin, 1999.

[19] R. D. James and M. Wuttig, *Magnetostriction of martensite*, Phil. Mag. A **77** (1998), 1273–1299.

[20] J. C. Kim, O. Y. Swon, and Z. H. Lee, *Unidirectional magnetostrictive terfenol/epoxy composite*, Appl. Phys. Lett. **84** (2004), 2130–2132.

[21] O. Y. Kwon, H. Y. Kim, S. I. Cha, and S. H. Hong, *Magnetostriction and magnetomechanical coupling of grain-aligned TbDyFe/epoxy-filled composites*, J. Appl. Phys. **97** (2005), 113905–1.4.

[22] A. A. Likhachev and K. Ullakko, *Magnetic-field-controlled twin boundaries motion and giant magneto-mechanical effects in NiMnGa shape memory alloy*, Phys. Lett. **A 275** (2000), 142–151.

[23] ———, *Quantitative model of large magnetostrain effect in ferromagnetic shape memory alloys*, Eur. Phys. J. B **14** (2000), 263–267.

[24] L. P. Liu, R. D. James, and P. H. Leo, *Magnetostrictive composites in the dilute limit*, J. Mech. Phys. Solids **54** (2006), 951–974.

[25] J. C. Maxwell, *Electricity and magnetism*, vol. 2, Claredon Press, Oxford, 1904.

[26] G. W. Milton, *The theory of composites*, Cambridge University Press, Cambridge, 2002.

[27] S. J. Murray, M. Marioni, S. M. Allen, R. C. O'Handley, and T. A. Lograsso, *6% magnetic-field-induced strain by twin-boundary motion in ferromagnetic Ni-Mn-Ga*, Appl. Phys. Lett. **77** (2000), 886–888.

[28] S. Müller, *Homogenization of nonconvex integral functionals and cellular elastic materials*, Arch. Rat. Mech. Anal. **99** (1987), 189–212.

[29] R. C. O'Handley, *Model for strain and magnetization in magnetic shape-memory alloys*, J. Appl. Phys. **83** (1998), 3263–3270.

[30] O. A. Oleinik, A. S. Shamaev, and G. A. Yosifian, *Mathematical problems in the theory of homogenization*, North-Holland, Amsterdam, 1992.

[31] S. W. Or et al., *Dynamic magnetomechanical properties of [112]-oriended Terfenol-D/epoxy 1-3 magnetostrictive particulate composites*, J. Appl. Phys. **93** (2003), 8510–812.

[32] J. A. Osborn, *Demagnetizing factors of the general ellipsoid*, Phys. Rev. **67** (1945), 351–357.

[33] Z. Peng et al., *Internal friction and modulus changes associated with martensitic and reverse transformations in a single crystal $Ni_{48.5}Mn_{31.4}Ga_{20.1}$ alloy*, J. Appl. Phys **95** (2004), 6960–6962.

[34] P. Ponte Castañeda and J. R. Willis, *The effect of spatial distribution on the effective behavior of composite materials and cracked media*, J. Mech. Phys. Solids **43** (1995), 1919–1951.

[35] L. Sandlund et al., *Magnetostriction, elastic moduli, and coupling factors of composite Terfenol-D*, J. Appl. Phys. **75** (1994), 5656–5658.

[36] M. Shanmugham, H. Bailey, and W. Armstrong, *Comparison of magnetostrictive performance loss of particulate $Tb_{0.3}Dy_{0.7}Fe_2$ epoxy composites prepared with different matrix polymers*, J. Mat. Res. **19** (2004), 795–805.

[37] M. Stipcich et al., *Elastic constants of Ni-Mn-Ga magnetic shape memory alloys*, Phys. Rev. B **70** (2004), 054115.

[38] O. Söderberg et al., *Recent breakthrough development of the magnetic shape memory effect in NiMnGa alloys*, Smart Mater. Struct. **14** (2005), S223–S235.

[39] R. Tickle, R.D. James, T. Shield, M. Wuttig, and V.V. Kokorin, *Ferromagnetic shape memory in the NiMnGa system*, IEEE Trans. Magn. **35** (1999), 4301–4310.

[40] K. Ullakko et al., *Magnetic-field-induced strains in polycrystalline Ni-Mn-Ga at room temperature*, Scripta Mat. **44** (2001), 475–480.

[41] K. Ullakko, J. K. Huang, C. Kantner, R. C. O'Handley, and V. V. Kokorin, *Large magnetic-field-induced strains in Ni_2MnGa single crystals*, Appl. Phys. Lett. **69** (1996), 1966–1968.

[42] D. Wand, J.-S. Chen, and L. Sun, *Homogenization of magnetostrictive particle-filled elastomers using an interface-enriched reproducing kernel particle method*, Fin. Elem. in Analysis and Design **39** (2003), 765–782.

[43] J. R. Willis, *Variational and related methods for the overall properties of composites*, Adv. Appl. Mech. **21** (1981), 1–78.

Bestellungen nimmt entgegen:

Institut für Angewandte Mathematik
der Universität Bonn
Sonderforschungsbereich 611
Wegelerstr. 6
D - 53115 Bonn

Telefon: 0228/73 4882
Telefax: 0228/73 7864
E-mail: link@wiener.iam.uni-bonn.de http://www.iam.uni-bonn.de/sfb611/

Verzeichnis der erschienenen Preprints ab No. 275

275. Otto, Felix; Reznikoff, Maria G.: Slow Motion of Gradient Flows

276. Albeverio, Sergio; Baranovskyi, Oleksandr; Pratsiovytyi, Mykola; Torbin, Grygoriy: The Ostrogradsky Series and Related Probability Measures

277. Albeverio, Sergio; Koroliuk, Volodymyr; Samoilenko, Igor: Asymptotic Expansion of Semi-Markov Random Evolutions

278. Frehse, Jens; Kassmann, Moritz: Nonlinear Partial Differential Equations of Fourth Order under Mixed Boundary Conditions

279. Juillet, Nicolas: Geometric Inequalities and Generalized Ricci Bounds in the Heisenberg Group

280. DeSimone, Antonio; Grunewald, Natalie; Otto, Felix: A New Model for Contact Angle Hysteresis

281. Griebel, Michael; Oeltz, Daniel: A Sparse Grid Space-Time Discretization Scheme for Parabolic Problems

282. Fattler, Torben; Grothaus, Martin: Strong Feller Properties for Distorted Brownian Motion with Reflecting Boundary Condition and an Application to Continuous N-Particle Systems with Singular Interactions

283. Giacomelli, Lorenzo; Knüpfer, Hans: Flat-Data Solutions to the Thin-Film Equation Do Not Rupture

284. Barbu, Viorel; Marinelli, Carlo: Variational Inequalities in Hilbert Spaces with Measures and Optimal Stopping

285. Philipowski, Robert: Microscopic Derivation of the Three-Dimensional Navier-Stokes Equation from a Stochastic Interacting Particle System

286. Dahmen, Wolfgang; Kunoth, Angela; Vorloeper, Jürgen: Convergence of Adaptive Wavelet Methods for Goal-Oriented Error Estimation; erscheint in: ENUMATH 2005 Proceedings

287. Maes, Jan; Kunoth, Angela; Bultheel, Adhemar: BPX-Type Preconditioners for 2nd and 4th Order Elliptic Problems on the Sphere; erscheint in: SIAM J. Numer. Anal.

288. Albeverio, Sergio; Mazzucchi, Sonia: Theory and Applications of Infinite Dimensional Oscillatory Integrals

289. Holtz, Markus; Kunoth, Angela: B-Spline Based Monotone Multigrid Methods, with an Application to the Pricing of American Options

290. Albeverio, Sergio; Ayupov, Shavkat A.; Kudaybergenov, Karim K.: Non Commutative Arens Algebras and their Derivations

291. Albeverio, Sergio; De Santis, Emilio: Reconstructing Transition Probabilities of a Markov Chain from Partial Observation in Space

292. Albeverio, Sergio; Hryniv, Rostyslav; Mykytyuk, Yaroslav: Inverse Spectral Problems for Bessel Operators

293. Albeverio, Sergio; Hryniv, Rostyslav; Mykytyuk, Yaroslav: Reconstruction of Radial Dirac Operators

294. Abels, Helmut; Kassmann, Moritz: The Cauchy Problem and the Martingale Problem for Integro-Differential Operators with Non-Smooth Kernels

295. Albeverio, Sergio; Daletskii, Alexei; Kalyuzhnyi, Alexander: Random Witten Laplacians: Traces of Semigroups, L^2-Betti Numbers and Index

296. Barlow, Martin T.; Bass, Richard F.; Chen, Zhen-Qing; Kassmann, Moritz: Non-Local Dirichlet Forms and Symmetric Jump Processes

297. Kassmann, Moritz: Harnack Inequalities. An Introduction; erscheint in: Boundary Value Problems

298. Berkels, Benjamin; Burger, Martin; Droske, Marc; Nemitz, Oliver; Rumpf, Martin: Cartoon Extraction based on Anisotropic Image Classification; erscheint in: Vision, Modeling, and Visualization Proceedings

299. Conti, Sergio; Lenz, Martin; Rumpf, Martin: Modeling and Simulation of Magnetic Shape-Memory Polymer Composites